Durable tumor regression in genetically altered malignant rhabdoid tumors by inhibition of methyltransferase EZH2

Sarah K. Knutson[1], Natalie M. Warholic[1], Tim J. Wigle, Christine R. Klaus, Christina J. Allain, Alejandra Raimondi, Margaret Porter Scott, Richard Chesworth, Mikel P. Moyer, Robert A. Copeland, Victoria M. Richon[2], Roy M. Pollock, Kevin W. Kuntz, and Heike Keilhack[3]

Epizyme, Inc., Cambridge, MA 02139

Edited* by Stuart H. Orkin, Children's Hospital and the Dana Farber Cancer Institute, Harvard Medical School and Howard Hughes Medical Institute, Boston, MA, and approved March 28, 2013 (received for review February 28, 2013)

Inactivation of the switch/sucrose nonfermentable complex component *SMARCB1* is extremely prevalent in pediatric malignant rhabdoid tumors (MRTs) or atypical teratoid rhabdoid tumors. This alteration is hypothesized to confer oncogenic dependency on EZH2 in these cancers. We report the discovery of a potent, selective, and orally bioavailable small-molecule inhibitor of EZH2 enzymatic activity, (N-((4,6-dimethyl-2-oxo-1,2-dihydropyridin-3-yl)methyl)-5-(ethyl (tetrahydro-2H-pyran-4-yl)amino)-4-methyl-4′-(morpholinomethyl)-[1,1′-biphenyl]-3-carboxamide). The compound induces apoptosis and differentiation specifically in *SMARCB1*-deleted MRT cells. Treatment of xenograft-bearing mice with (N-((4,6-dimethyl-2-oxo-1,2-dihydropyridin-3-yl)methyl)-5-(ethyl(tetrahydro-2H-pyran-4-yl)amino)-4-methyl-4′-(morpholinomethyl)-[1,1′-biphenyl]-3-carboxamide) leads to dose-dependent regression of MRTs with correlative diminution of intratumoral trimethylation levels of lysine 27 on histone H3, and prevention of tumor regrowth after dosing cessation. These data demonstrate the dependency of *SMARCB1* mutant MRTs on EZH2 enzymatic activity and portend the utility of EZH2-targeted drugs for the treatment of these genetically defined cancers.

epigenetic cancer therapy | EZH2 inhibitor

Posttranslational modifications of core histone proteins of chromatin play important roles in controlling the fidelity of gene transcription patterns in cells (1). Paramount among these transcription-controlling modifications is methylation events at lysine and arginine residues, catalyzed by histone methyltransferases (HMTs) (2). EZH2 is the catalytic subunit of the multiprotein HMT complex known as polycomb repressive complex 2 (PRC2), catalyzing the methylation of lysine 27 of histone H3 (H3K27); trimethylation of H3K27 leads to repression of gene expression (3). EZH2 has been implicated in several cancer types by mutation, amplification, and/or overexpression (4). For instance, heterozygous *EZH2* mutations at residues within the catalytic (Su[var]3-9, enhancer of zeste, trithorax) (SET) domain have been observed in 10% of non-Hodgkin lymphomas and can drive H3K27 hypertrimethylation, abnormal gene expression, and lymphomagenesis. We and others previously reported that selective inhibition of EZH2 results in selective killing of lymphoma cells bearing *EZH2* mutations, suggesting that EZH2 enzymatic activity is a required driver of proliferation in the mutant-bearing cells (5–7).

Gene expression is also regulated by remodeling of nucleosomes in an ATP-dependent manner (8). Of the ATP-dependent chromatin remodelers, switch/sucrose nonfermentable (SWI/SNF) complexes are emerging as bona fide tumor suppressors, as specific inactivating mutations in several SWI/SNF subunits are found in human cancers (9). For instance, the SMARCB1 subunit (also known as SNF5, INI1, or BAF47) is inactivated via biallelic mutations in nearly all malignant rhabdoid tumors (MRTs) and atypical teratoid rhabdoid tumors (ATRTs), aggressive cancers of young children with no effective therapy (10). Gene expression and functional studies in cell culture demonstrated that SMARCB1 loss leads to decreased expression of cell cycle inhibitors (11), tumor suppressors like *BIN1* (12), and genes of neuronal differentiation (13, 14), while hedgehog and MYC pathway genes were up-regulated (14, 15). Homozygous *SMARCB1* knockout mice are embryonically lethal, but *SMARCB1*-heterozygous mice are viable and develop sarcomas that closely resemble human MRTs with the second allele of *SMARCB1* spontaneously lost (16). *SMARCB1*-conditional inactivation in T cells leads to fully penetrant T-cell lymphomas at a median age of onset of 11 wk (17). Interestingly, tumorigenesis can be completely suppressed by tissue-specific codeletion of *EZH2*, suggesting an antagonistic interaction between PRC2 and SWI/SNF. Indeed, *EZH2* expression is elevated in primary *SMARCB1*-deficient tumors, and polycomb target genes are also broadly repressed in such tumors as well as in *SMARCB1* knockout mouse embryonic fibroblasts.

Through iterative medicinal chemistry, we have developed a selective EZH2 inhibitor with favorable pharmacological properties. The compound was used to test whether *SMARCB1*-deleted MRTs are selectively sensitive to EZH2 inhibition in vitro and in vivo, which would suggest new treatment modalities for such genetically defined cancer types.

Results

EPZ-6438 Is a Potent and Selective Inhibitor of EZH2. High-throughput screening afforded a pyridone-containing EZH2 inhibitor series (5), and through iterative medicinal chemistry, we developed (N-((4,6-dimethyl-2-oxo-1,2-dihydropyridin-3-yl)methyl)-5-(ethyl (tetrahydro-2H-pyran-4-yl)amino)-4-methyl-4′-(morpholinomethyl)-[1,1′-biphenyl]-3-carboxamide) (EPZ-6438) (Fig. 1*A*), a compound with superior potency and pharmacokinetic properties relative to our previously described tool compound 1-cyclopentyl-N-((4,6-dimethyl-2-oxo-1,2-dihydropyridin-3-yl)methyl)-6-(4-(morpholinomethyl) phenyl)-1H-indazole-4-carboxamide (5) (EPZ005687). EPZ-6438 inhibited the activity of human PRC2-containing wild-type EZH2 with an inhibition constant (K_i) value of 2.5 ± 0.5 nM, and similar potency was observed for EZH2 proteins bearing all known

Author contributions: S.K.K., R.C., M.P.M., V.M.R., K.W.K., and H.K. designed research; S.K.K., N.M.W., T.J.W., and H.K. performed research; C.R.K., C.J.A., A.R., and K.W.K. contributed new reagents/analytic tools; S.K.K., N.M.W., T.J.W., M.P.S., R.C., M.P.M., R.A.C., V.M.R., R.M.P., K.W.K., and H.K. analyzed data; and S.K.K., R.A.C., R.M.P., and H.K. wrote the paper.

Conflict of interest statement: All authors except V.M.R. are employees of Epizyme, Inc.

*This Direct Submission article had a prearranged editor.

Freely available online through the PNAS open access option.

[1]S.K.K. and N.M.W. contributed equally to this work.

[2]Present address: Department of Oncology, Sanofi, Cambridge, MA 02139.

[3]To whom correspondence should be addressed. E-mail: hkeilhack@epizyme.com.

This article contains supporting information online at www.pnas.org/lookup/suppl/doi:10.1073/pnas.1303800110/-/DCSupplemental.

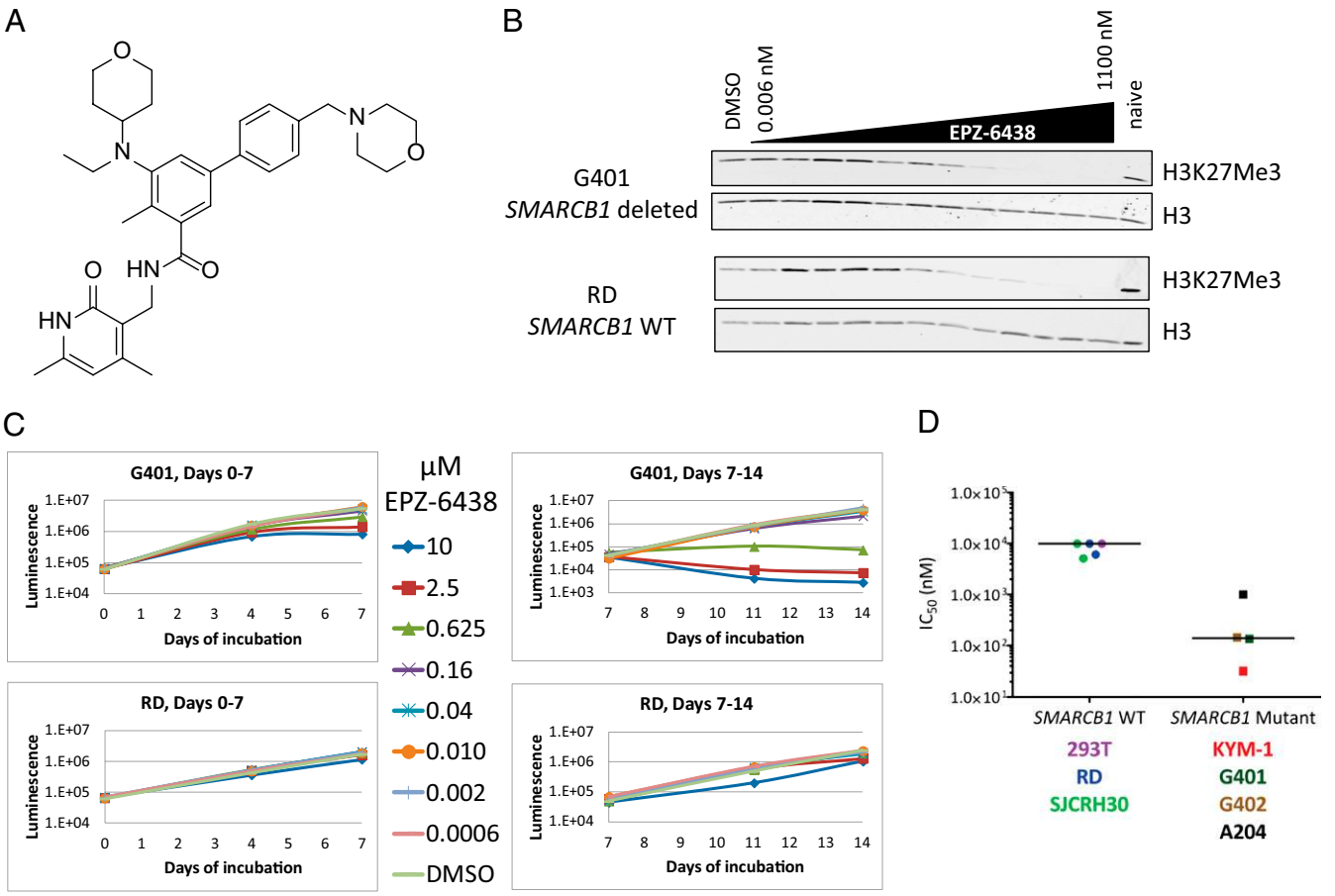

Fig. 1. Effects of EPZ-6438 on cellular global histone methylation and cell viability. (*A*) Chemical structure of EPZ-6438. (*B*) Concentration-dependent inhibition of cellular H3K27Me3 levels in G401 and RD cells. (*C*) Selective inhibition of proliferation of *SMARCB1*-deleted G401 cells by EPZ-6438 in vitro (measured by ATP content). G401 and RD cells were replated at the original seeding densities on day 7. Each point represents the mean for each concentration (n = 3). (*D*) Proliferation IC_{50} values (day 14) for *SMARCB1* wild-type and mutant cells. Compound incubations for each experiment were performed in triplicate, and symbols represent the mean of two experiments for all cell lines. The horizontal lines represent the median. Mean calculation of duplicate experiments was not possible for RD and SJCRH30 cells; individual values are shown (Table S2).

lymphoma change-of-function mutations (Table S1). As previously described for EPZ005687 (5), steady-state analysis of the enzyme kinetics revealed that the present compound, EPZ-6438, inhibits EZH2 in a manner competitive with the substrate *S*-adenosylmethionine (SAM) (that is, EPZ-6438 and SAM binding to EZH2 is mutually exclusive, such that only one or the other ligand can bind but both cannot bind to the enzyme simultaneously) (Fig. S1*A*), and noncompetitive with the peptide or nucleosome substrate (that is, EPZ-6438 binding is not mutually exclusive or synergistic with binding of the peptide/nucleosome substrate of the enzymatic reactions) (Fig. S1*B*) (18). We also assessed inhibition by EPZ-6438 against a panel of HMTs other than EZH2 encompassing both lysine and arginine HMTs. EPZ-6438 displayed a 35-fold selectivity versus EZH1 and >4,500-fold selectivity relative to 14 other HMTs tested (Table S1). These in vitro properties (i.e., mechanism of action, specificity, cellular potency) of EPZ-6438

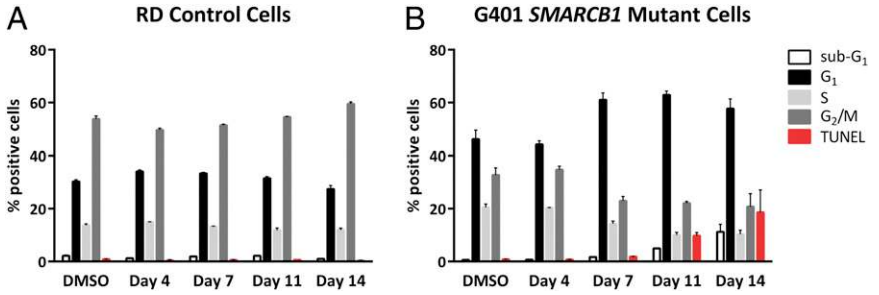

Fig. 2. EPZ-6438 induces G_1 arrest and apoptosis in *SMARCB1*-deleted MRT cells. Cell cycle analysis (by flow cytometry) and determination of apoptosis (by TUNEL assay) in RD (*A*) or G401 cells (*B*) during incubation with either vehicle or 1 μM EPZ-6438 for up to 14 d. G_1 arrest was observed as of day 7, and apoptosis was induced as of day 11. Data are represented as mean values ± SEM (n = 2). The DMSO control values shown are the average ± SEM from each time point. Cells were split and replated on days 4, 7, and 11 at the original seeding density.

are similar to those of other published EZH2 inhibitors (6, 7). Additionally, EPZ-6438, has demonstrated good oral bioavailability in animals, making EPZ-6438 particularly useful for in vivo studies.

EPZ-6438 Specifically Inhibits Cellular H3K27 Methylation Leading to Selective Apoptotic Killing of SMARCB1 Mutant MRT Cells. A panel of *SMARCB1*-deficient MRT cells and *SMARCB1* wild-type control cells (confirmed by immunoblot; Fig. S2*A*) were treated with EPZ-6438 for 4 d, resulting in concentration-dependent reductions in global H3K27Me3 levels (Fig. 1*B* and Table S2). Treatment of either wild-type or mutant cells resulted in diminution of H3K27 methylation, whereas other histone methyl marks were unaffected (Fig. S2*B*). In vitro treatment of *SMARCB1*-deleted MRT cell lines with EPZ-6438 induced strong antiproliferative effects with IC_{50} values in the nanomolar range, whereas the control (wild-type) cell lines were minimally affected (Fig. 1 *C* and *D* and Table S2). Antiproliferative effects were apparent in *SMARCB1*-deleted MRT cells after 7 d of compound exposure, but required 14 d of exposure for maximal activity. We also assessed the effects of incubation with EPZ-6438 (1 μM) for 14 d on cell cycle progression and apoptosis in G401 and RD cells. EPZ-6438 incubation of RD (*SMARCB1* wild-type) cells showed no changes in cell cycle or apoptosis compared with the DMSO control (Fig. 2*A*). In contrast, G401 (*SMARCB1*-deleted) cells showed an increase in the percentage of cells in G_1 phase, and a concomitant decrease in S phase and G_2/M phase after 7 d (Fig. 2*B*). There was no apparent increase in the sub-G_1 fraction through day 7, suggesting that apoptosis was not yet induced by that time. This coincides with the growth curves of G401 cells in the presence of EPZ-6438 that display cytotoxicity only after 7 d of incubation (Fig. 1*C*). Following EPZ-6438 treatment of G401 cells for up to 14 d, the fraction of cells in sub-G_1 as well as apoptotic cells determined by TUNEL assay increased in a time-dependent manner through days 11 and 14, indicating that EPZ-6438–mediated cell death occurred through the induction of apoptosis (Fig. 2*B*).

EPZ-6438 Induces Genes of Neuronal Differentiation and Cell Cycle Inhibition While Suppressing Expression of Hedgehog Pathway Genes, MYC and EZH2. It has been suggested that SMARCB1 loss drives cancer formation through simultaneous epigenetic perturbation of key cancer pathways (19). We confirmed the previously described reduced expression of genes important for neuronal differentiation (*CD133*, *DOCK4*, *PTPRK*), cell cycle inhibition (*CDKN2A*), and tumor suppression (*BIN1*), as well as increased expression of the hedgehog pathway gene *GLI1* in *SMARCB1*-deleted G401 cells compared with control cells (Fig. 3*A*). EPZ-6438 treatment of G401 cells for up to 7 d strongly induced expression of *CD133*, *DOCK4*, and *PTPRK* and up-regulated cell cycle inhibitors

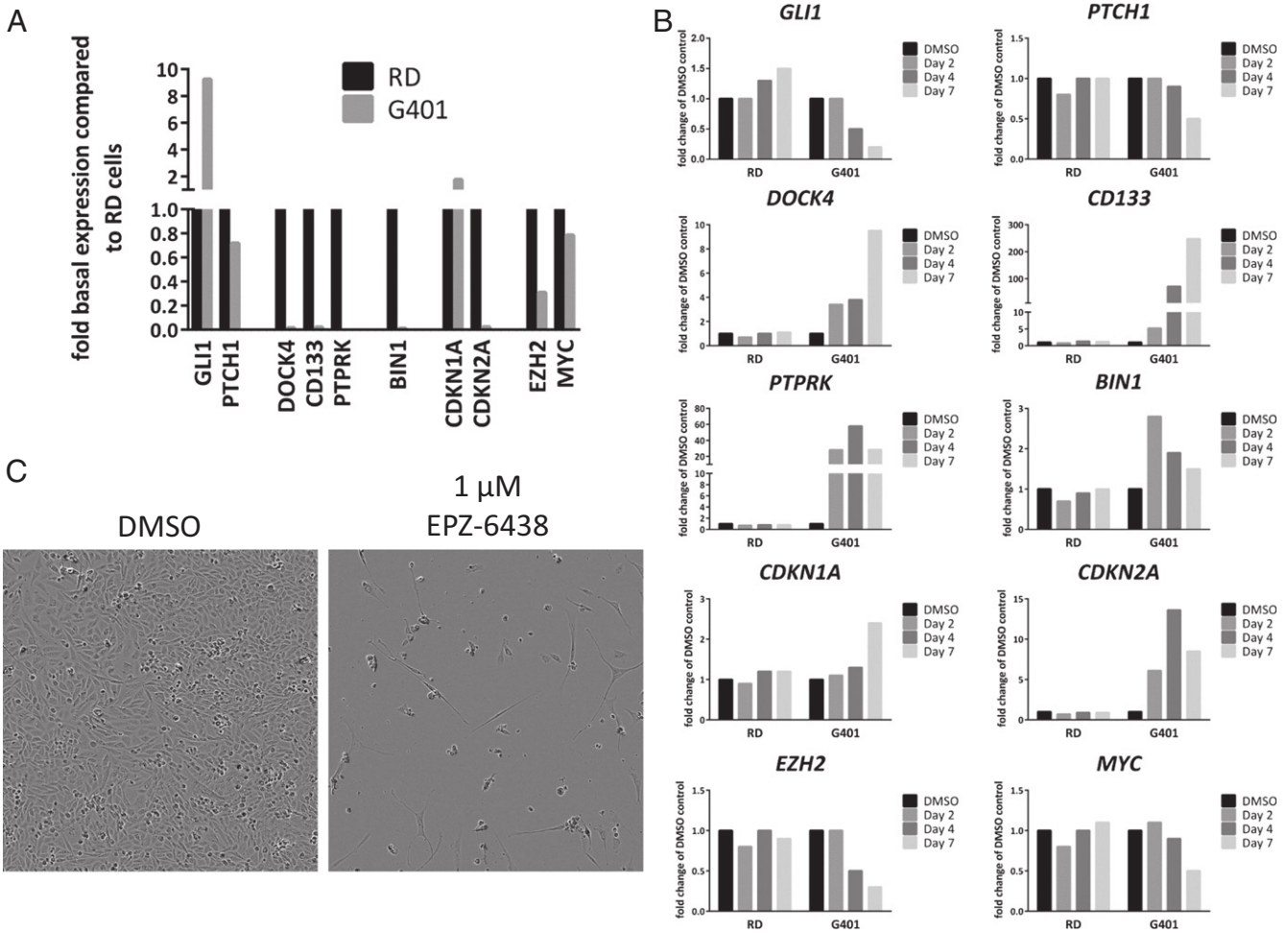

Fig. 3. EPZ-6438 induces changes in expression of SMARCB1-regulated genes and cell morphology. (*A*) Basal expression of SMARCB1-regulated genes in G401 *SMARCB1*-deleted cells, relative to RD control cells [measured by quantitative PCR (qPCR); $n = 2$]. (*B*) G401 and RD cells were incubated with either DMSO or 1 μM EPZ-6438 for 2, 4, and 7 d. Gene expression was determined by qPCR ($n = 2$) and is expressed relative to the DMSO control of each time point. (*C*) G402 cells were incubated with either DMSO (*Left*) or 1 μM EPZ-6438 (*Right*) for 14 d. Cells were split and replated to the original seeding density on day 7.

CDKN1A and *CDKN2A* and tumor suppressor *BIN1*, all in a time-dependent manner (Fig. 3*B*). At least one of these genes (*CDKN2A*) is known to be a direct target of PRC2 repression (17). EPZ-6438 also down-regulated the expression of hedgehog pathway genes *MYC* and *EZH2* over the same time period. Concomitant with these transcriptional changes, we additionally observed morphological changes in another *SMARCB1*-deleted cell line, G402. When exposed to EPZ-6438 for 14 d, the G402 cells (but not the G401 cells) assumed a neuron-like morphology (Fig. 3*C* and Fig. S3). In contrast, EPZ-6438 incubation of RD control cells had minimal effects on expression of the above-mentioned genes or on cell morphology.

EPZ-6438 Leads to Complete and Sustained Regression of SMARCB1 Mutant MRT Xenografts. A study in SCID mice bearing s.c. G401 xenografts was performed where animals were dosed orally for 21 d with EPZ-6438. One-half of the mice per group were euthanized on day 21 to collect blood and tissues, while the remaining animals were treated for an additional 7 d and then left without dosing for another 32 d. EPZ-6438 was well tolerated at all doses with minimal effect on body weight (Fig. S4*A*). Oral dosing at 250 or 500 mg/kg twice daily (BID) for 21–28 d practically eliminated the fast-growing G401 tumors (Fig. S4 *B* and *C* and Fig. 4*A*). Regrowth was not observed for 32 d after dose cessation. EPZ-6438 dosed at 125 mg/kg induced tumor stasis during the administration period and produced a significant tumor growth delay compared with vehicle after the dosing period. Measuring EPZ-6438 plasma levels either 5 min before or 3 h after dosing on day 21 revealed a clear dose-dependent increase in systemic exposure (Fig. S4*D*). Tumors that were harvested from subsets of mice from each group on day 21 showed strong inhibition of H3K27Me3, correlating with the antitumor activity (maximum effect achieved at 250 mg/kg;

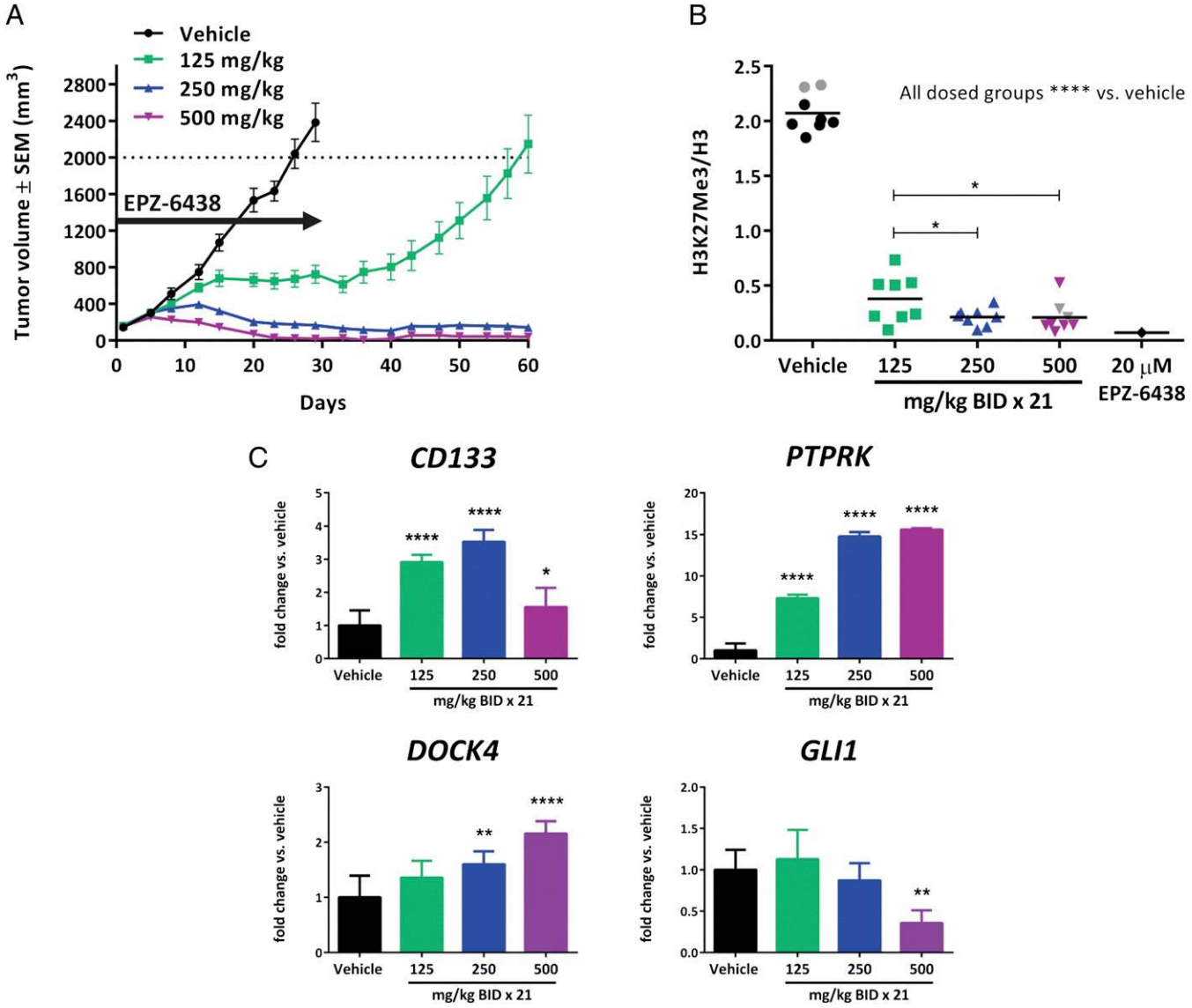

Fig. 4. EPZ-6438 eradicates *SMARCB1*-deleted MRT xenografts in SCID mice. (*A*) Tumor regressions induced by twice daily (BID) administration of EPZ-6438 for 28 d at the indicated doses. Compound administration was stopped on day 28, and tumors were allowed to regrow until they reached 2,000 mm^3 (data shown as mean values ± SEM; $n = 8$). (*B*) EZH2 target inhibition in G401 xenograft tumor tissue collected from mice euthanized on day 21. Each point shows the ratio of H3K27Me3 to total H3, measured by ELISA. The horizontal lines represent group mean values; gray symbols are values outside of the ELISA standard curve. (*C*) Change in gene expression in G401 xenograft tumor tissue collected from mice treated with EPZ-6438 for 21 d. Data are presented as fold change compared with vehicle ± SEM ($n = 6$, $n = 4$ for 500 mg/kg group). $^*P < 0.05$, $^{**}P < 0.01$, $^{****}P < 0.0001$, vs. vehicle, Fisher's exact test.

Fig. 4*B*). In addition, dose-dependent changes in the expression of *CD133*, *PTPRK*, *DOCK4*, and *GLI1* were detected in the G401 xenograft tumors (Fig. 4*C*).

Discussion

MRTs and ATRTs are extremely aggressive pediatric cancers of the brain, kidney, and soft tissues that are highly malignant, locally invasive, frequently metastatic, and particularly lethal (10). They are typically diploid and lack genomic aberrations; however, they are characterized by an almost complete penetrance of loss of SMARCB1, a core component of the SWI/SNF chromatin remodeling complex (20). The biallelic inactivation of *SMARCB1* is in essence the sole genetic event in MRTs and ATRTs, which suggests a driver role for this genetic aberration. Through genetic studies, it has been suggested that PRC2 and SWI/SNF antagonistically regulate gene expression around several pathways including RB, Cyclin D1, MYC (19), and hedgehog (15). Analyses of rhabdoid tumor tissue and functional studies suggest that such cancers may originate from early stem cells where chromatin around specific genes remains dominated by PRC2 histone markings (14). At the time of differentiation, absence of SMARCB1 in rhabdoid tumors prevents the de-repression of such genes (which would normally occur in the *SMARCB1* wild-type setting), leading to aberrant activation of proliferation, survival, and self-renewal pathways and oncogenesis. These results provide a successful testing of the hypothesis that pharmacological inhibition of EZH2 enzymatic activity would provide a basis for therapeutic intervention in MRTs and ATRTs. In the present report, we show that pharmacological inhibition of EZH2 induced antiproliferative effects specifically in *SMARCB1*-deleted MRT cell lines and led to complete regressions of MRT xenografts in mice without any regrowth for the full duration of the study. These data confirm the dependency of such cancers on PRC2 activity, despite the fact that EZH2 itself is not genetically altered in this context. Our results in MRT cell culture are similar to findings by Alimova et al. (21) showing that disruption of EZH2 by RNAi and/or 3-Deazaneplanocin A (DZNep, an indirect and general inhibitor of methyltransferases) impairs ATRT cell growth. Interpretation of cellular phenotypes caused by DZNep, however, is complicated by its ability to reduce methylation levels at multiple histone residues targeted by HMTs other than EZH2.

Numerous studies show that reconstitution of SMARCB1 into MRT or ATRT cells restores the abnormal gene expression pattern (for instance by increasing expression of cell cycle inhibitors and tumor suppressors) and leads to impaired cell growth (22). Here, we show that, in the context of *SMARCB1*-deleted MRT, inhibition of EZH2 functions as a SMARCB1 surrogate and derepresses neuronal differentiation genes, cell cycle inhibitors, and tumor suppressors while reducing *GLI1*, *PTCH1*, *MYC*, and *EZH2*. The sum of the effects of EPZ-6438–mediated EZH2 inhibition on several cancer pathways is likely the cause for the dramatic and permanent antitumor activity seen in MRT models. This suggests that EPZ-6438 may represent a new and exciting potential treatment modality for these lethal childhood tumors. Furthermore, because several members of the SWI/SNF complex are genetically altered in other cancer types besides MRT, it is conceivable that EZH2 may also play a role in tumor maintenance and survival in a spectrum of cancer types. Combined with recent reports demonstrating the effectiveness of EZH2 inhibitors in selective killing of *EZH2* mutant bearing non-Hodgkin lymphomas, the present data suggest that small-molecule–based inhibition of EZH2 may be an effective mechanism of therapeutic intervention in a variety of hematologic and solid tumors for which genetic alterations—either target-directed or indirect—confer a proliferative dependency on EZH2 enzymatic activity.

Materials and Methods

Synthesis of EPZ-6438. A synthetic route of EPZ-6438 is described in patent cooperation treaty (PCT) patent application publication number WO/2012/142504.

Biochemical Methods. Methods to assay HMT activities were performed as previously described (5).

Cell Culture. 293T (CRL-11268), RD (CRL-136), SJCRH30 (CRL-2061), A204 (HTB-82), G401 (CRL-1441), and G402 (CRL-1440) were obtained from ATCC. KYM-1 (JCRB0627) was obtained from JCRB. 293T and RD cells were cultured in DMEM plus 10% (vol/vol) FBS. SJCRH30 cells were cultured in RPMI plus 10% (vol/vol) FBS. A204, G401, and G402 cells were cultured in McCoys 5a plus 10% (vol/vol) FBS. KYM-1 cells were cultured in DMEM/Ham's F-12 plus 10% (vol/vol) FBS.

Western Blots Analysis. Histones were acid extracted as previously described (23). Western blots for acid-extracted histones were performed as previously described (5). Western blot conditions for whole-cell lysates are described in *SI Text*.

In Vitro Cell Assays. For the adherent cell line proliferation assays [all cell lines except KYM-1, which was analyzed as previously described for suspension cell lines (22)], plating densities for each cell line were determined based on growth curves (measured by ATP content) and density over a 7-d time course. On the day before compound treatment, cells were plated in either 96-well plates in triplicate (for the day 0–7 time course) or 6-well plates (for replating on day 7 for the remainder of the time course). On day 0, cells were either untreated, DMSO-treated, or treated with EPZ-6438 starting at 10 μM and decreasing in either threefold or fourfold dilutions. Plates were read on day 0, day 4, and day 7 using Cell Titer Glo (Promega), with compound/media being replenished on day 4. On day 7, the six-well plates were trypsinized, centrifuged, and resuspended in fresh media for counting by Vi-Cell. Cells from each treatment were replated at the original density in 96-well plates in triplicate. Cells were allowed to adhere to the plate overnight, and cells were treated as on day 0. On days 7, 11, and 14, plates were read using Cell Titer Glo, with compound/media being replenished on day 11. Averages of triplicates were used to plot proliferation over the time course, and calculate IC_{50} values. For cell cycle and apoptosis, G401 and RD cells were plated in 15-cm dishes in duplicate at a density of 1×10^6 cells per plate. Cells were incubated with EPZ-6438 at 1 μM, in a total of 25 mL, over a course of 14 d, with cells being split back to original plating density on day 4, 7, and 11. Cell cycle analysis and TUNEL assay were performed using a Guava flow cytometer, following the manufacturer's protocol.

Gene Expression Analysis. G401 and RD cells were plated in T-75 flasks at 175,000 cells per flask and 117,000 cells per flask, respectively, and allowed to adhere overnight. On day 0, cells were treated in duplicates with DMSO or 1 μM EPZ-6438. Cells were harvested and pelleted on days 2, 4, and 7 with media and compound being replenished on day 4. Tumor tissue from the G401 xenograft animals dosed for 21 d [vehicle, 125 mg/kg, and 250 mg/kg (six animals each) and 500 mg/kg (four animals) EPZ-6438 dose groups] were used for gene expression analysis. Total mRNA was extracted from cell pellets and tumor tissue using the RNeasy Mini Kit (Qiagen; 74106) and reverse transcribed by the High Capacity cDNA Reverse Transcription Kit [Applied Biosystems (AB); 4368813]. RT-PCR was performed by ViiA 7 Real-Time PCR Systems (AB) using TaqMan Fast Advanced Master Mix (AB; 4444964) and TaqMan primer/probe sets (*SI Materials and Methods*). Gene expression was normalized to 18S (AB; Hs99999901_s1), and fold change was calculated using the ΔΔCt method. For the in vivo samples, the average Ct value ± SD was determined for each dose group and fold change compared with vehicle dose group was calculated using the ΔΔCt method.

Measurement of H3K27 Methylation in Tumor Tissue. Histones were isolated from tumors as previously described (23) and were prepared in coating buffer (PBS with 0.05% BSA). Two independent ELISAs were performed using antibodies specific for H3K27Me3 (CST; 9733) or total H3 (Abcam; ab1791), and ratios for H3K27Me3 to total H3 were calculated. The detailed procedure is described in *SI Text*.

Xenograft Study. All of the procedures related to animal handling, care, and treatment in this study were performed according to the guidelines approved by the Institutional Animal Care and Use Committee of Shanghai Chempartner following the guidance of the Association for Assessment and Accreditation of Laboratory Animal Care. For the in vivo study, mice were inoculated s.c. at the right flank with G401 tumor cells (5×10^6 cells per mouse) in 0.2-mL mixture of base media and Matrigel (McCoy's 5A/Matrigel, 1:1) for tumor development. The treatments were started when the tumor size reached ~157 mm^3 for the tumor efficacy study (n = 16 mice per group). EPZ-6438 or vehicle (0.5% NaCMC plus 0.1% Tween 80 in water) was administered orally BID at a dose

volume of 10 μL/g for either 21 or 28 d. Animal body weights were measured every day during the first week, and then twice weekly for the remainder of the study. Tumor size was measured twice weekly in two dimensions using a caliper, and the volume was expressed in cubic millimeters. For pharmacokinetic–pharmacodynamic analysis, eight mice with the largest tumor burden were euthanized for tumor and blood collection after 21 d of dosing. The remaining mice continued dosing for 1 more week, and from day 29, treatment was stopped and the mice were enrolled in a tumor growth delay study. Mice were observed as individuals until they reached the tumor weight endpoint (2,000 mm^3) or until day 60 (whichever came first).

1. Rando OJ (2012) Combinatorial complexity in chromatin structure and function: Revisiting the histone code. *Curr Opin Genet Dev* 22(2):148–155.
2. Richon VM, et al. (2011) Chemogenetic analysis of human protein methyltransferases. *Chem Biol Drug Des* 78(2):199–210.
3. Margueron R, Reinberg D (2011) The polycomb complex PRC2 and its mark in life. *Nature* 469(7330):343–349.
4. Chase A, Cross NC (2011) Aberrations of EZH2 in cancer. *Clin Cancer Res* 17(9):2613–2618.
5. Knutson SK, et al. (2012) A selective inhibitor of EZH2 blocks H3K27 methylation and kills mutant lymphoma cells. *Nat Chem Biol* 8(11):890–896.
6. McCabe MT, et al. (2012) EZH2 inhibition as a therapeutic strategy for lymphoma with EZH2-activating mutations. *Nature* 492(7427):108–112.
7. Qi W, et al. (2012) Selective inhibition of Ezh2 by a small molecule inhibitor blocks tumor cells proliferation. *Proc Natl Acad Sci USA* 109(52):21360–21365.
8. Hargreaves DC, Crabtree GR (2011) ATP-dependent chromatin remodeling: Genetics, genomics and mechanisms. *Cell Res* 21(3):396–420.
9. Wilson BG, Roberts CW (2011) SWI/SNF nucleosome remodellers and cancer. *Nat Rev Cancer* 11(7):481–492.
10. Ginn KF, Gajjar A (2012) Atypical teratoid rhabdoid tumor: Current therapy and future directions. *Front Oncol* 2:114.
11. Kia SK, Gorski MM, Giannakopoulos S, Verrijzer CP (2008) SWI/SNF mediates polycomb eviction and epigenetic reprogramming of the INK4b-ARF-INK4a locus. *Mol Cell Biol* 28(10):3457–3464.
12. McKenna ES, et al. (2012) Epigenetic inactivation of the tumor suppressor BIN1 drives proliferation of SNF5-deficient tumors. *Cell Cycle* 11(10):1956–1965.
13. Albanese P, Belin MF, Delattre O (2006) The tumour suppressor hSNF5/INI1 controls the differentiation potential of malignant rhabdoid cells. *Eur J Cancer* 42(14): 2326–2334.
14. Gadd S, Sredni ST, Huang CC, Perlman EJ; Renal Tumor Committee of the Children's Oncology Group (2010) Rhabdoid tumor: Gene expression clues to pathogenesis and potential therapeutic targets. *Lab Invest* 90(5):724–738.
15. Jagani Z, et al. (2010) Loss of the tumor suppressor Snf5 leads to aberrant activation of the Hedgehog-Gli pathway. *Nat Med* 16(12):1429–1433.
16. Roberts CW, Galusha SA, McMenamin ME, Fletcher CD, Orkin SH (2000) Haploinsufficiency of Snf5 (integrase interactor 1) predisposes to malignant rhabdoid tumors in mice. *Proc Natl Acad Sci USA* 97(25):13796–13800.
17. Wilson BG, et al. (2010) Epigenetic antagonism between polycomb and SWI/SNF complexes during oncogenic transformation. *Cancer Cell* 18(4):316–328.
18. Copeland RA (2013) *Evaluation of Enzyme Inhibitors in Drug Discovery: A Guide for Medicinal Chemists and Pharmacologists* (Wiley, Hoboken, NJ), 2nd Ed.
19. Roberts CW, Biegel JA (2009) The role of SMARCB1/INI1 in development of rhabdoid tumor. *Cancer Biol Ther* 8(5):412–416.
20. Lee RS, et al. (2012) A remarkably simple genome underlies highly malignant pediatric rhabdoid cancers. *J Clin Invest* 122(8):2983–2988.
21. Alimova I, et al. (2013) Inhibition of EZH2 suppresses self-renewal and induces radiation sensitivity in atypical rhabdoid teratoid tumor cells. *Neuro Oncol* 15(2):149–160.
22. Sansam CG, Roberts CW (2006) Epigenetics and cancer: Altered chromatin remodeling via Snf5 loss leads to aberrant cell cycle regulation. *Cell Cycle* 5(6):621–624.
23. Daigle SR, et al. (2011) Selective killing of mixed lineage leukemia cells by a potent small-molecule DOT1L inhibitor. *Cancer Cell* 20(1):53–65.